Analytic approximations to the strengths of near-threshold optical Feshbach resonances

Mateusz Borkowski

Department of Physics, Columbia University, 538 West 120th Street, New York, New York 10027-5255, USA;
Van der Waals-Zeeman Institute, Institute of Physics, University of Amsterdam, Science Park 904, 1098 XH Amsterdam, The Netherlands;
and Institute of Physics, Faculty of Physics, Astronomy and Informatics, Nicolaus Copernicus University,
Grudziadzka 5, 87-100 Torun, Poland

(Received 11 March 2023; accepted 22 May 2023; published 1 June 2023)

Optical Feshbach resonances allow one to control cold atomic scattering, produce ultracold molecules, and study atomic interactions via photoassociation spectroscopy. In the limit of ultracold s-wave collisions, the strength of an optical Feshbach resonance can be expressed via an energy-independent parameter called the optical length. Here we give fully analytic approximate expressions for its magnitude applicable to near-threshold bound states of an excited molecular state dominated by a single resonant-dipole or van der Waals interaction. We express these magnitudes in terms of intuitive quantities, such as the laser intensity, the excited-state binding energy, the s-wave scattering length, and the Condon point. Additionally, we extend the utility of the optical length to associative stimulated Raman adiabatic passage in three-dimensional optical lattices by showing that the free-bound Rabi frequency induced by a laser coupling a pair of atoms in an optical lattice site can be approximately related to the trap frequency and the optical length.

DOI: 10.1103/PhysRevA.107.063101

I. INTRODUCTION

Feshbach resonances [1] emerge in cold atomic collisions when the entrance scattering channel is coupled to a discrete molecular state by, e.g., hyperfine mixing. Optical Feshbach resonances (OFRs) [2] are created artificially by a laser tuned nearby an electronically excited molecular bound state. The unavoidable losses due to spontaneous decay from the excited state are the foundation of photoassociation spectroscopy: an essential tool for studying weakly bound states in homonuclear [3–13] and heteronuclear molecules composed of the colliding species [14–17]. For several systems, most notably ^{88}Sr [18], the decay from the excited bound state may efficiently produce ultracold ground-state molecules [18–23]. Finally, OFRs can control the scattering length [24–32] with high spatial and temporal resolution [30].

The strength of an s-wave OFR can be expressed by an optical length $l_{\rm opt}$ [2,25,33,34] related to a free-bound Franck-Condon factor between the ground-state scattering and excited bound-state wave functions. These can be evaluated numerically by solving the appropriate radial Schrödinger equations. Alternatively, the Franck-Condon factors can be approximated using the well-known reflection approximation originally devised by Jabłoński in the context of his quantum theory of spectral line broadening [35] and later appropriated for cold collisions by Julienne [36]. The major virtue of the reflection approximation is that it relates the strength of a photoassociation line to the squared ground-state wave function at the outermost Condon point (Fig. 1), a point where the incident photon's energy matches the energy difference between ground- and excited-state potential, and thus can, e.g., explain gaps in photoassociation spectra as due to nodes in the ground-state wave function. The reflection approximation works well when the excited-state potential has a much longer range than the ground-state potential, for instance, when the excited state is dominated by a strong resonant-dipole interaction. An improved version of the reflection formula, the stationary phase approximation [34], has an extended range of validity that also covers van der Waals (vdW) excited states so long as the excited-state vdW interaction is much stronger than the ground state's. In practice, however, to use either formula one still must compute the ground-state wave function numerically (see, e.g., [37–39]), estimate the excited-state vibrational splittings, and, for the stationary phase formula, numerically integrate a WKB phase shift, often lacking knowledge of the relevant interatomic potentials. This may require postulating a model potential without prior experimental input. Then, calculating, e.g., the dependence of the photoassociation spectra on the scattering length would require further manual tuning of that potential.

In this paper we evaluate the reflection [36,40] and stationary phase formulas [34] (where appropriate) using the WKB approximation to arrive at fully analytic formulas for the strengths of optical Feshbach resonances that require no numerical solutions to the radial Schrödinger equation. To do so, we will consider the excited-state interaction potential $V_e(R)$ as dominated by a single $-C_n^e R^{-n}$ term, where R is the internuclear distance. In particular, we will consider two useful limiting cases: (i) an excited state with a strong resonant-dipole interaction $V_e \sim -C_3^e R^{-3}$, which describes homonuclear collisions in a laser field tuned near either an allowed or a sufficiently strong intercombination transition, and (ii) a vdW excited state $V_e \sim -C_6^e R^{-6}$, which describes heteronuclear systems. We will express $l_{\rm opt}$ using intuitive physical quantities: the s-wave scattering length a, leading interaction terms (C_3^e or C_6^e), the excited-state binding energy E_b, the Condon point R_C, and the classical outer turning point R_t. In particular, the explicit connection to the scattering length

could help experimentalists choose the best isotopologue of a system via mass scaling [41–43]. We will test our formulas on real-world examples: intercombination line OFRs in Yb_2 (a system whose excited-state interactions are dominated by a resonant-dipole R^{-3} term) [12,29,44,45] and OFRs in the Rb + Sr system near the Rb $D1$ line [46] (which has a van der Waals R^{-6} tail in the excited-state interaction potential). Despite approximating real atomic interactions with just one dominant $C_n R^{-n}$ term, we will find that the resultant fully analytic formulas can still match numerical computations semiquantitatively.

Finally, given the interest in the production of molecules from atomic pairs in three-dimensional (3D) optical lattice sites [47,48], we will show how the free-bound Rabi frequency $\Omega_{\rm FB}$ for the transition of an unbound atomic pair state in an optical lattice site to the excited molecular bound state can be calculated from the optical length $l_{\rm opt}$ and then test it using $^{84}Sr_2$ experimental data [13,48]. Our formula, based on ideas from quantum defect theory [49], corroborates the empirical observation [48] that the free-bound Rabi frequency scales approximately with the optical lattice frequency $\omega_{\rm trap}$ as $\Omega_{\rm FB} \propto \omega_{\rm trap}^{3/4}$.

II. DERIVATION OF THE ANALYTIC FORMULAS

Here we analytically evaluate optical lengths within the reflection approximation [36,50] and its more accurate version, the stationary phase approximation [34], by using the WKB approximation. In Sec. II A we will define the optical length in terms of a free-bound Franck-Condon factor and in Sec. II B we will quote the reflection and stationary phase approximations for that Franck-Condon factor. In the following sections we will look at the individual terms that comprise these approximations and evaluate them one by one. For the ratio of vibrational spacings and potential slope (Sec. II C) we will employ the Le Roy–Bernstein formula [51] allowing us to write them in terms the dominant excited-state interaction and the excited bound-state position. Then, in Sec. II D we will introduce the three models of the ground-state wave function in the zero-energy limit, i.e., the asymptotic, long-range, and short-range models, that allow us to write the wave function in terms of the ground-state s-wave scattering length and the ground-state van der Waals coefficients C_6^g and optionally C_8^g. In Sec. II E we will tackle the extra phase correction term that differentiates between the reflection [36] and stationary phase [34] approximations by using the WKB approximation on locally linearized excited-state potential. In Sec. II F we list the final analytic formulas: Eqs. (21a)–(22c).

A. Optical length

Consider an ultracold collision of two atoms, in an s wave, at a kinetic energy E, and described by an energy-normalized scattering wave function f_g. The strength of an OFR, or its ability to induce observable photoassociative losses or a useful change to the scattering length, is commonly expressed via an optical length, defined as [2,25,33,34]

$$l_{\rm opt} = \frac{\Gamma_{\rm stim}}{2k\gamma_m}. \tag{1}$$

Here γ_m is the decay rate of the excited bound state and $\hbar\Gamma_{\rm stim} = 2\pi|\langle f_g|V^{\rm opt}|\psi_b\rangle|^2$ is a stimulated rate [50] induced by coupling an excited bound state ψ_b to the ground-state scattering wave function f_g, via a matrix element $V_{\rm opt}$ that describes the interaction of the colliding atoms with light. For a laser detuned by δ, the change to scattering length Δa and the photoassociative inelastic collision rate $K_{\rm in}$ [2,12,13,25,31,52,53] are

$$\Delta a = \frac{l_{\rm opt}\gamma_m\delta}{\delta^2 + (\eta\gamma_m)^2/4}, \tag{2}$$

$$K_{\rm in} = g\frac{2\pi\hbar}{\mu}\frac{l_{\rm opt}\eta\gamma_m^2}{\delta^2 + \gamma_m^2(\eta + 2kl_{\rm opt})^2/4}, \tag{3}$$

where γ_m is the natural linewidth of the excited bound state, $\eta \geqslant 1$ is a broadening factor that accounts for other loss processes, μ is the reduced mass, g is a symmetry factor (2 for a thermal gas of identical bosons and 1 otherwise), and the wave number $k = \sqrt{2\mu E}/\hbar$ at collision energy E.

In this paper we consider optical Feshbach resonances close to near-threshold excited molecular bound states where the molecular dipole transition moment and the molecular state decay rate γ_m can be expressed in terms of the properties of the constituent atoms. In such a case it is well known [33,45,50,53–56] that the optical length becomes

$$l_{\rm opt} = \frac{3\lambda_a^3}{16\pi c} I f_{\rm rot}\frac{|\langle f_g|\psi_b\rangle|^2}{k}, \tag{4}$$

where I is the laser intensity (hereafter assumed equal to 1 W/cm^2), λ_a is the atomic transition wavelength, and $f_{\rm rot}$ is a rotational Hönl-London factor stemming from translating the electric-field operator from space-fixed to body-fixed coordinates [54,57]. Within the Wigner threshold regime the amplitude of the ground-state scattering wave function f_g is proportional to $\sqrt{k}$, making $l_{\rm opt} \sim f_g^2/k$ practically constant with respect to collision energy. Thus $l_{\rm opt}$ may be evaluated in the limit of zero energy and used for all collision energies in a sufficiently cold gas [53].

B. Reflection and stationary phase approximations

The starting point for the present paper is the stationary phase approximation formula [34,36,50] for the Franck-Condon factor which, in this paper, we will further evaluate using WKB approximations. The full derivation of the stationary phase formula can be found in Ref. [34]; here we will only briefly outline the derivation.

The regular wave functions for the ground- and excited-state potentials can be written in the Milne form

$$\psi_b(R) = \left(\frac{\partial E_b}{\partial v}\right)^{1/2}\left(\frac{2\mu}{\pi\hbar^2}\right)^{1/2}\alpha_e(R)\sin[\beta(R)], \tag{5}$$

$$f_g(R) = \left(\frac{2\mu}{\pi\hbar^2}\right)^{1/2}\alpha_g(R)\sin[\phi(R)], \tag{6}$$

where $\alpha_g(R)$ and $\alpha_e(R)$ are the local amplitudes of the ground- and excited-state wave functions, respectively, and $\phi(R)$ and $\beta(R)$ are their respective phases. Thus, the desired Franck-

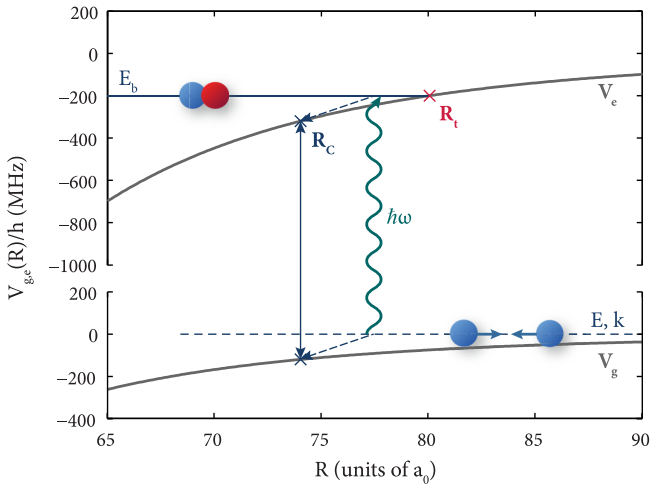

FIG. 1. In an optical Feshbach resonance the initial atomic scattering state, characterized by a collision energy E and wave vector k, are coupled by the incident photon $\hbar\omega$ to an excited molecular bound state at energy E_b. Here V_g and V_e are the ground- and excited-state potentials, respectively, R_t is the classical outer turning point of the excited bound state, and R_C is the outermost Condon point, the internuclear distance where the photon energy matches exactly the energy difference between the ground- and excited-state potentials.

Condon factor

$$|\langle f_g|\psi_b\rangle|^2 = \frac{\partial E_b}{\partial \nu}\left(\frac{2\mu}{\pi\hbar^2}\right)^2 |I_{eg}|^2 \tag{7}$$

can be written in terms of the following integral:

$$I_{eg} = \int_0^\infty dR\alpha_e(R)\alpha_g(R)\sin[\beta(R)]\sin[\phi(R)]. \tag{8}$$

The oscillating terms can be rewritten as $\sin[\beta(R)]\sin[\phi(R)] = \{\cos[\beta(R)-\phi(R)] - \cos[\beta(R)+\phi(R)]\}/2$. The fast oscillating second term contributes little to the integral and can be omitted.

The crux of the stationary phase approximation lies in the observation that the main contribution to this integral stems from the stationary phase point where $\partial\beta(R)/\partial R - \partial\phi(R)/\partial R \approx 0$. Within the WKB approximation the respective derivatives are $\beta(R)/\partial R \approx \sqrt{2\mu[E_b - V_e(R)]} = k_e(R)$ and $\phi(R)/\partial R \approx \sqrt{-2\mu[V_g(R)]} = k_g(R)$ and the stationary point becomes the Condon point (Fig. 1), defined as the outermost point R_C where $V_e(R_C) - E_b = V_g(R_C)$. Additionally, while the entirety of the ground-state wave function cannot be described by the WKB approximation (see Sec. II D), the phase and amplitude of the excited-state wave function for $R < R_t$ can be well approximated by $\alpha_e(R) = \{2\mu[E_b - V_e(R)]\}^{-1/4}$ and $\beta(R) = -\pi/4 - \Delta\beta(R, R_t)$ with the phase integral $\Delta\beta(R, R_t) = \int_R^{R_t} dR' k_e(R')$, with R_t the classical outer turning point.

In the final step of the derivation, the phase difference is expanded to second order around the Condon point R_C,

$$\phi(R) - \beta(R) \approx b_0 + b_1(R - R_C) + \frac{b_2}{2}(R - R_C)^2, \tag{9}$$

where $b_0 = \phi(R_C) + \Delta\beta(R_C, R_t) + \pi/4$, $b_1 \approx 0$, and $b_2 \approx \mu D_C/\hbar^2 k_e(R_C)$ [34]. Here the slope difference at the Condon point $D_C = V_e'(R_C) - V_g'(R_C)$. Finally, the integral can be evaluated assuming that the amplitudes $\alpha_{g,e}$ are slowly varying around the Condon point [34,50]:

$$\begin{aligned} I_{eg} &\approx \frac{1}{2}\int_0^\infty dR\alpha_e(R)\alpha_g(R)\cos\left(b_0 + \frac{b_2}{2}(R - R_C)^2\right) \\ &\approx \frac{1}{2}\alpha_e(R_C)\alpha_g(R_C)\sqrt{\frac{2\pi}{b_2}}\cos\left(b_0 + \frac{\pi}{4}\right) \\ &\approx -\sqrt{\frac{\pi\hbar^2}{2\mu D_C}}\alpha_g(R_C)\sin[\phi(R_C) + \Delta\beta(R_C, R_t)]. \end{aligned} \tag{10}$$

The final approximate Franck-Condon factor can be written as a product of four terms [34]

$$|\langle f_g|\psi_b\rangle|^2 \approx \frac{\partial E_b}{\partial \nu}\frac{1}{D_C}|f_g(R_C)|^2 \times \frac{\sin^2[\phi(R_C) + \Delta\beta(R_C, R_t)]}{\sin^2[\phi(R_C)]}. \tag{11}$$

In this work we will aim to analytically approximate these terms. The first term $\partial E_b/\partial\nu$ is the local vibrational spacing in the excited state. The second depends on the difference D_C between the excited- and ground-state potential slopes taken at the Condon point R_C: $D_C = V_e'(R_C) - V_g'(R_C)$. We will treat the two together in Sec. II C. The third term is the squared ground-state wave function at the Condon point. The last is a phase correction term [34] that will improve our model for the more deeply bound states where the difference between R_C and the classical outer turning point R_t can be substantial. For very weakly bound states of a resonant-dipole system the Condon point R_C is very close the outer turning point R_t and Eq. (11) reduces to the well-known reflection approximation [35,36,40,50]

$$|\langle f_g|\psi_b\rangle|^2 \approx \frac{\partial E_b}{\partial \nu}\frac{1}{D_C}|f_g(R_C)|^2. \tag{12}$$

The stationary phase approximation works best when the two molecular potentials V_e and V_g are very different; while in the resonant-dipole case this is usually true unless the resonant-dipole interaction is very weak, for vdW systems this implies an excited-state interaction coefficient C_6^e significantly larger than the ground state C_6^g [34].

C. Vibrational spacing and potential slopes

In our quest towards simple expressions we will benefit from two main observations. First, the Le Roy–Bernstein theory [51,58] provides a formula for the vibrational spacing in a $-C_nR^{-n}$ potential,

$$\frac{\partial E_b}{\partial \nu} = \hbar\sqrt{\frac{2\pi}{\mu}}\frac{\Gamma(1+1/n)}{\Gamma(1/2+1/n)}\frac{n}{C_n^{1/n}}(-E_b)^{(n+2)/2n}, \tag{13}$$

where $\Gamma(x)$ is the Euler gamma function and E_b is the resonance position. When the OFR laser is on resonance and the collision energy $E \to 0$, the difference in potentials at the Condon point matches the bound-state energy $V_e(R_C) - V_g(R_C) = E_b$. We can write the potential difference in terms of multipole expansions $V_e - V_g = -C_3^eR^{-3} - \Delta C_6R^{-6} - \cdots$, where $\Delta C_6 = C_6^e - C_6^g$. To the lowest order, the appropriate

Condon points for the resonant-dipole and vdW systems are $R_C^{\text{r-d}} \approx (C_3^e)^{1/3}(-E_b)^{-1/3}$ and $R_C^{\text{vdW}} \approx \Delta C_6^{1/6}(-E_b)^{-1/6}$. Similarly, we may approximate the difference in potential slopes with $D_C^{\text{r-d}} \approx -3C_3R_C^{-4}$ and $D_C^{\text{vdW}} \approx -6\Delta C_6 R_C^{-7}$. With these choices the first two terms in Eq. (11) simplify to

$$\left(\frac{\partial E_b}{\partial \nu}\frac{1}{D_C}\right)^{\text{r-d}} \approx \hbar\sqrt{\frac{2\pi}{\mu}}\frac{\Gamma(4/3)}{\Gamma(5/6)}\frac{1}{\sqrt{-E_b}}, \tag{14a}$$

$$\left(\frac{\partial E_b}{\partial \nu}\frac{1}{D_C}\right)^{\text{vdW}} \approx \hbar\sqrt{\frac{2\pi}{\mu}}\frac{\Gamma(7/6)}{\Gamma(2/3)}\left(\frac{\Delta C_6}{C_6^e}\right)^{1/6}\frac{1}{\sqrt{-E_b}}. \tag{14b}$$

D. Zero-energy ground-state wave functions

The second simplification stems from the Wigner threshold law [2,45,53,59,60]: For sufficiently low collision energies, the ratio $|\langle f_g|\psi_b\rangle|^2/k$ is effectively constant, allowing us to evaluate f_g at zero energy, where simple analytic models are available. However, due to the breakdown of the WKB approximation near $R_{\text{vdW}} = (2\mu C_6^g/\hbar^2)^{1/4}/2$ [2,40], we will be forced to use separate wave-function models for the long-range ($R \gtrapprox R_{\text{vdW}}$) and short-range ($R \lessapprox R_{\text{vdW}}$) internuclear separations.

The asymptotic ($R \to \infty$) form of the s-wave scattering wave function [shown in Fig. 2(a)] is

$$f_g^{\text{asym}}(R) \sim \sqrt{\frac{2\mu}{\pi\hbar^2 k}}\sin(kR+\eta), \tag{15a}$$

where the phase shift η due to the short-range potential defines the scattering length via $a = \lim_{k\to 0} -\eta/k$. At internuclear distances closer to R_{vdW} the long-range van der Waals interaction causes the wave function to deviate from its asymptotic form. Reference [36] gives the approximate formula

$$f_g^{\text{long}}(R) \approx \sqrt{\frac{2\mu}{\pi\hbar^2 k}}\sin\left[k\left(R-a-\frac{8}{15}\frac{R_{\text{vdW}}^4}{R^3}\right)\right]\left(1-\frac{4}{5}\frac{R_{\text{vdW}}^4}{R^4}\right), \tag{15b}$$

which closely matches the numerical wave function for R ranging from $+\infty$ down to about R_{vdW} [Fig. 2(a)].

For short-range interatomic distances, i.e., $R \lessapprox R_{\text{vdW}}$, we will use a WKB wave function

$$f_g^{\text{short}}(R) \approx \sqrt{\frac{2\mu}{\pi\hbar^2}}A(R,E)C^{-1}(E)\sin[\phi(R,E)], \tag{15c}$$

where $A(R,E) = 1/\sqrt{k_{\text{local}}(R)}$ and $\phi(R,E)$ are the typical WKB amplitude and phase. Since we assumed that the ground-state potential $V_g(R) \sim -C_6^g R^{-6}$, the local wave number $k_{\text{local}} = [k^2 - 2\mu V(R)/\hbar^2]^{1/2}$ entering the expression for the WKB amplitude can be replaced with $k_{\text{local}} \approx (2\mu C_6^g/\hbar^2)^{1/2}R^{-3} = 4R_{\text{vdW}}^2 R^{-3}$. The additional term $C^{-1}(E) = \{k\bar{a}[1+(a/\bar{a}-1)^2]\}^{1/2}$ is a correction to the amplitude for near-threshold scattering wave functions [2,63,64]. The quantity $\bar{a} = 2^{-1/2}[\Gamma(3/4)/\Gamma(5/4)]R_{\text{vdW}} = (0.956)\ldots(R_{\text{vdW}})$ is the mean scattering length that enters the semiclassical formula for a in a vdW potential [41].

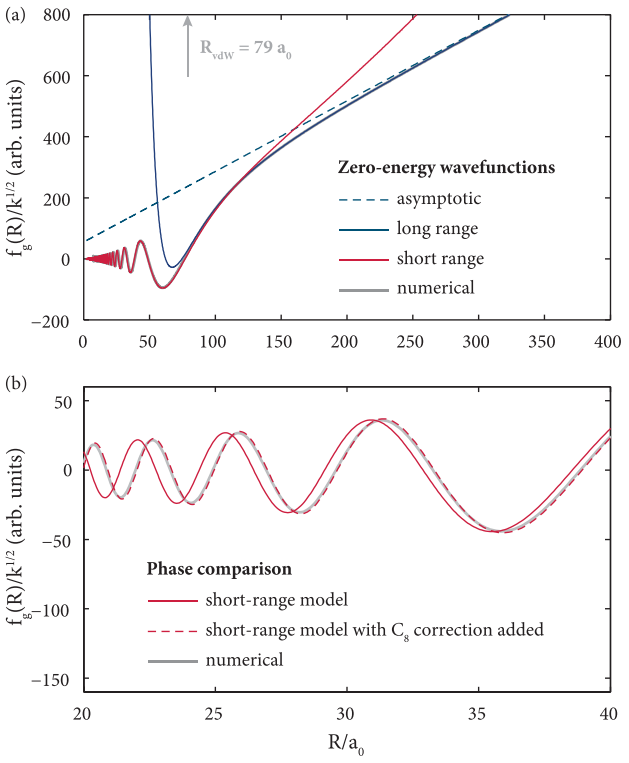

FIG. 2. Comparison of model zero-energy scattering wave functions on the example of $^{176}Yb_2$ ($a = -24a_0$ [61,62]). (a) Numerical wave function (thick gray line) approximated by the asymptotic wave function (16) (blue dashed line); its improved version, the long-range model of Ref. [36], Eq. (17) (blue solid line); and the WKB short-range wave function (18) (red solid line), respectively. (b) Comparison of the short-range WKB wave fuction (18), where the wave-function phase $\phi(R)$ is calculated without (red solid line) and with (red dashed line) the $\phi_8(R)$ phase correction (17c). A quick glance reveals that including the extra phase correction improves the agreement with the numerically obtained wave function.

The zero-energy WKB phase $\phi(R)$ can be related to the s-wave scattering length at its large-R limit $\phi_\infty = \int_{R_0}^{\infty} k_{\text{local}}(R')dR'$ that enters the well-known semiclassical formula $a = \bar{a}[1-\tan(\phi_\infty - 3\pi/8)]$ [41]. Thus we can very well start at infinite nuclear separation with the asymptotic value of ϕ_∞ obtained by inverting the semiclassical formula and accumulate the WKB phase inward. Since the Condon points R_C are well past the Le Roy radius [58], we can expand the ground-state potential as $V_g \approx -C_6^g R^{-6} - C_8^g R^{-8}$ and express the phase $\phi(R)$ as

$$\phi(R) = \phi_\infty - \phi_6(R) - \phi_8(R), \tag{16}$$

where the individual phase terms are

$$\phi_\infty = \frac{3\pi}{8} + \arctan\left(1-\frac{a}{\bar{a}}\right), \tag{17a}$$

$$\phi_6(R) = \int_R^\infty \left(\frac{2\mu C_6^g}{\hbar^2}R^{-6}\right)^{1/2}dR = 2\left(\frac{R_{\text{vdW}}}{R}\right)^2, \tag{17b}$$

$$\phi_8(R) = \frac{1}{8}\frac{\sqrt{2\mu}}{\hbar}\frac{C_8^g}{\sqrt{C_6^g}}R^{-4}. \tag{17c}$$

The term ϕ_6 is the exact WKB phase due to just the R^{-6} tail. The next van der Waals term $-C_8^g R^{-8}$ can be accounted for perturbatively. A first-order WKB phase correction due to a small additional potential δV on top of a potential V may be expressed as [65]

$$\delta\phi \approx \frac{1}{2}\int_{R_C}^{\infty} \frac{\sqrt{2\mu}}{\hbar}\frac{\delta V}{\sqrt{|V(R)|}}dR. \tag{18}$$

The expression for ϕ_8 is obtained by assuming the $\delta V = -C_8 R^{-8}$ contribution is much smaller than the $V = -C_6 R^{-6}$ term. While ϕ_6 alone may be sufficient for many applications, taking the C_8 term into account significantly improves the model wave function at shorter internuclear separations, as shown in Fig. 2(b). Finally, in the zero-energy ($k \to 0$) limit we have

$$\left|\frac{f_g^2(R_C)}{k}\right|^{\text{asym}} \approx \frac{2\mu}{\pi\hbar^2}(R_C - a)^2, \tag{19a}$$

$$\left|\frac{f_g^2(R_C)}{k}\right|^{\text{long}} \approx \frac{2\mu}{\pi\hbar^2}\left(R_C - a - \frac{8}{15}\frac{R_{\text{vdW}}^4}{R_C^3}\right)^2 \times \left(1 - \frac{4}{5}\frac{R_{\text{vdW}}^4}{R_C^4}\right)^2, \tag{19b}$$

$$\left|\frac{f_g^2(R_C)}{k}\right|^{\text{short}} \approx \frac{2\mu}{\pi\hbar^2}\bar{a}\left[1 + \left(\frac{a}{\bar{a}} - 1\right)^2\right] \times \frac{R_C^3}{4R_{\text{vdW}}^2}\sin^2[\phi(R_C)]. \tag{19c}$$

We note that while the simple asymptotic expression only reproduces the outermost node of the scattering wave function (and only for a large positive scattering length), it will turn out useful for transitions to weakly bound states supported by a strong resonant-dipole interaction whose Condon points are usually well past R_{vdW}. The short-range model is a rapidly oscillating function due to the $\sin^2[\phi(R_C)]$ term and is appropriate for vdW systems and more deeply bound states in the resonant-dipole case. The typical values of R_{vdW} range from about $30a_0$ to about $100a_0$ [2].

E. WKB phase correction

The last term in Eq. (11) adds an excited-state WKB phase correction $\Delta\beta(R_C; R_t) = \int_{R_C}^{R_t}[2\mu(E_b - V_e)/\hbar^2]^{1/2}dR$ [34] that improves upon the reflection approximation for deeply bound states. For this reason, we will only use it in conjunction with the short-range wave-function model [Eq. (15c)]. We can obtain an approximate analytic solution to this integral by simply linearizing V_e around the classical outer turning point R_t. Since by definition at the turning point $V_e(R_t) = E_b$, we can approximate $V_e(R)$ as $V_e(R) \approx E_b + V_e'(R_t)(R - R_t)$. For the resonant-dipole case

$$[\Delta\beta]^{\text{r-d}} \approx \frac{\sqrt{2\mu C_3^e}}{\hbar}\frac{2\sqrt{3}}{3}R_t^{-2}(R_t - R_C)^{3/2}, \tag{20a}$$

whereas for a van der Waals system

$$[\Delta\beta]^{\text{vdW}} \approx \frac{\sqrt{2\mu C_6^e}}{\hbar}\frac{2\sqrt{6}}{3}R_t^{-7/2}(R_t - R_C)^{3/2}. \tag{20b}$$

The distance between the turning and Condon points itself $R_t - R_C$ can be estimated as follows. The turning point is defined as a point where the excited-state potential matches the bound-state energy: $V_e(R_t) = E_b$. The position of the Condon point additionally depends on the ground-state potential: $V_e(R_C) - V_g(R_C) = E_b$. In a vdW system, if one ignores any potential terms other than C_6, then $R_t = (-C_6^e/E_b)^{1/6}$ and $R_C = (-\Delta C_6/E_b)^{1/6}$. For a resonant-dipole system with a dominant $-C_3^e R^{-3}$ excited-state interaction we can start from the definitions of R_C and R_t to obtain, after some algebra,

$$R_t = R_C\left(1 - \frac{C_6^g R_C^{-3}}{C_3^e}\right)^{-1/3} \approx R_C\left(1 + \frac{C_6^g R_C^{-3}}{3C_3^e}\right),$$

and hence $R_t - R_C \approx C_6^g R_C^{-3}/3C_3^e$. Finally we can, without losing much accuracy, replace the R_C on the right-hand side with R_t so that $R_t - R_C \approx C_6^g R_t^{-3}/3C_3^e$.

F. Final formulas

Combining the formulas for resonant-dipole vibrational spacing [Eq. (14a)] with the asymptotic [Eq. (19a)] and long-range wave-function models [Eq. (19b)], respectively, produces the following approximate expressions:

$$l_{\text{opt}}^{\text{r-d,asym}} = \frac{3\lambda_a^3}{16\pi c}If_{\text{rot}}\frac{2\sqrt{2\mu}}{\hbar\sqrt{\pi}}\frac{\Gamma(4/3)}{\Gamma(5/6)}\frac{1}{\sqrt{-E_b}}(R_C - a)^2, \tag{21a}$$

$$l_{\text{opt}}^{\text{r-d,long}} = \frac{3{\lambda_a}^3}{16\pi c}If_{\text{rot}}\frac{2\sqrt{2\mu}}{\hbar\sqrt{\pi}}\frac{\Gamma(4/3)}{\Gamma(5/6)}\frac{1}{\sqrt{-E_b}} \times \left(R_C - a - \frac{8}{15}\frac{R_{\text{vdW}}^4}{R_C^3}\right)^2\left(1 - \frac{4}{5}\frac{R_{\text{vdW}}^4}{R_C^4}\right)^2. \tag{21b}$$

It is worth pointing out that in the limit of $R \gg R_{\text{vdW}}$ the long-range formula reduces to the asymptotic one.

To obtain the short-range expression we similarly combine the formula for the vibrational spacing [Eq. (14a)], but with the short-range (WKB) wave function [Eq. (19c)], and, in this case, also take into account the WKB phase correction [Eq. (11)]. This has the effect of replacing the $\sin^2[\phi(R_C)]$ term in the model wave function with an appropriate $\sin^2[\phi(R_C) + \Delta\beta(R_C, R_t)]$ term:

$$l_{\text{opt}}^{\text{r-d,short}} = \frac{3\lambda_a^3}{16\pi c}If_{\text{rot}}\frac{2\sqrt{2\mu}}{\hbar\sqrt{\pi}}\frac{\Gamma(4/3)}{\Gamma(5/6)}\frac{1}{\sqrt{-E_b}}\bar{a} \times \left[1 + \left(\frac{a}{\bar{a}} - 1\right)^2\right]\frac{R_C^3}{4R_{\text{vdW}}^2}\sin^2[\phi(R_C) + \Delta\beta(R_C, R_t)]. \tag{21c}$$

Similar formulas for a van der Waals–dominated excited state can be constructed analogously and the final

formulas are

$$l_{\rm opt}^{\rm vdW,asym} = \frac{3\lambda_a^3}{16\pi c} I f_{\rm rot} \frac{2\sqrt{2\mu}}{\hbar\sqrt{\pi}} \frac{\Gamma(7/6)}{\Gamma(2/3)} \left(\frac{\Delta C_6}{C_6^e}\right)^{1/6} \times \frac{1}{\sqrt{-E_b}} (R_C - a)^2, \tag{22a}$$

$$l_{\rm opt}^{\rm vdW,long} = \frac{3\lambda_a^3}{16\pi c} I f_{\rm rot} \frac{2\sqrt{2\mu}}{\hbar\sqrt{\pi}} \frac{\Gamma(7/6)}{\Gamma(2/3)} \left(\frac{\Delta C_6}{C_6^e}\right)^{1/6} \times \frac{1}{\sqrt{-E_b}} \left(R_C - a - \frac{8}{15}\frac{R_{\rm vdW}^4}{R_C^3}\right)^2 \times \left(1 - \frac{4}{5}\frac{R_{\rm vdW}^4}{R_C^4}\right), \tag{22b}$$

$$l_{\rm opt}^{\rm vdW,short} = \frac{3\lambda_a^3}{16\pi c} I f_{\rm rot} \frac{2\sqrt{2\mu}}{\hbar\sqrt{\pi}} \frac{\Gamma(7/6)}{\Gamma(2/3)} \left(\frac{\Delta C_6}{C_6^e}\right)^{1/6} \times \frac{1}{\sqrt{-E_b}} \bar{a}\left[1 + \left(\frac{a}{\bar{a}} - 1\right)^2\right] \frac{R_C^3}{4R_{\rm vdW}^2} \sin^2 \times [\phi(R_C) + \Delta\beta(R_C, R_t)]. \tag{22c}$$

III. EXAMPLES

Now we can proceed to testing our approximations. To test the formulas for the resonant dipole case, we will use the example of intercombination line photoassociation of Yb_2 [44,45]. For the van der Waals case we will look at photoassociation near the $D1$ line of Rb in the Rb + Sr system [23,46].

A. A resonant-dipole case: Intercombination line photoassociation in Yb

Our first example is a resonant-dipole-dominated case of photoassociation near the ${}^1S_0 \to {}^3P_1$ transition of Yb [44,45]. The excited ${}^1S_0 \to {}^3P_1$ asymptote supports four Hund's case (c) molecular states with the projection of electronic angular momentum on the internuclear axis $|\Omega| = 0, 1$ and with gerade (g) and ungerade (u) symmetry. By the Laporte rule only electric dipole transitions to the u excited states are possible from the g electronic ground state. The long-range interaction in the excited electronic state is dominated by the resonant-dipole terms

$$C_{3,0}^e = \frac{3}{2}\frac{\hbar}{\tau_A}\left(\frac{\lambda_A}{2\pi}\right)^3 \tag{23}$$

for the $|\Omega| = 0$ state and $C_{3,1}^e = -C_{3,0}^e/2$ for the $|\Omega| = 1$ state. Here τ_A and λ_A are the excited-state lifetime and transition wavelength, respectively. The resonant-dipole interaction is strongly repulsive in the 1_u, state leaving $0_u{}^+$ as the only molecular state supporting a series of bound states near the dissociation limit. From an s-wave collision only excited states with total angular momentum $J_e = 1$ can be reached.

Figure 3 shows optical lengths of intercombination line OFRs in the resonant-dipole-dominated Yb system. The numerical optical lengths were calculated using previous ground- [62] and excited-state models [45] using the Colbert-Miller discrete-variable representation (DVR) method [38] with a variable grid [39]. Both the excited- and ground-state wave functions were calculated using the DVR method. For

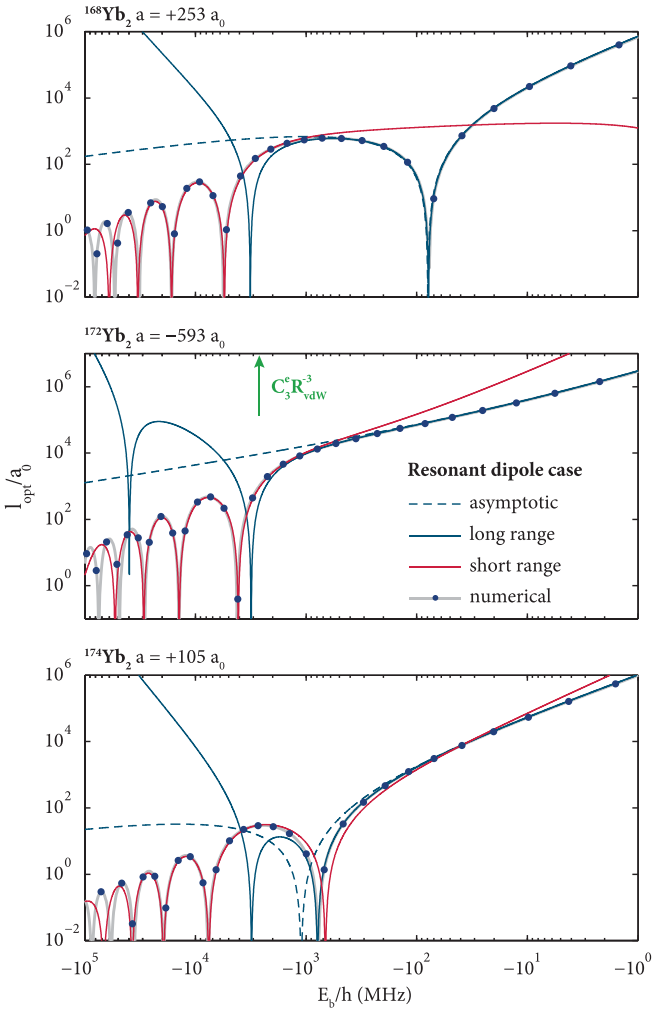

FIG. 3. Optical lengths in a resonant-dipole-dominated system on the example of intercombination-line OFRs in Yb [44,45]. Dots represent excited bound states. The gray lines connecting the dots were interpolated by scaling the quantum defect in the excited-state potential. The blue dashed and solid lines denote the asymptotic and long-range models (21a) and (21b), respectively. The red lines denote the short-range model (21c). The asymptotic and long-range models match the numerical results down to about −1 and −2 GHz detuning, respectively. The enhanced modeling of the ground-state wave function [36] employed in the long-range model improves the agreement compared to the asymptotic model. For larger detunings the short-range model utilizing the WKB ground-state wave function correctly reproduces the numerical optical lengths satisfactorily down to about −20 GHz, beyond which the positions of nodes are no longer correct. A more detailed error plot for the $^{174}Yb_2$ case (bottom panel) is shown in Fig. 5(a).

the scattering wave function we picked the lowest solution above the dissociation limit, which we found to be energetically well within the Wigner threshold law. This enabled us to calculate the Franck-Condon factor in Eq. (4) as a simple vector dot product between the DVR matrix eigenvectors.

The ground-state potential is based on *ab initio* calculations [66] with fitted long-range parameters $C_6^g \approx 1937 E_h a_0^6$ and $C_8^g \approx (2.265 \times 10^5) E_h a_0$ (E_h and a_0 are the atomic units

of energy and length). The scattering lengths for the ^{168}Yb, ^{172}Yb, and ^{174}Yb isotopes are $253a_0$, $-593a_0$, and $105a_0$, respectively [61,62]. The van der Waals length is $R_{\rm vdW} \approx 78a_0$ and the mean scattering length $\bar{a} \approx 74a_0$. For the excited state we use a Lennard $-$ Jones $+ C_8$ potential model [45] where the $C_3^e \approx 0.1949E_h a_0^3$ is calculated from Eq. (23) using the lifetime $\tau_A = 869.6$ ns ($\gamma_a = 2\pi \times 183$ kHz) and the transition wavelength $\lambda_a = 555.8$ nm. The rotational Hönl-London factor is $f_{\rm rot} = \frac{1}{3}$ [45,53,55] and the excited state has an added rotational interaction energy $V_{\rm rot} = (\hbar^2/2\mu R^2)$ $[J_e(J_e+1)+2]$ [67].

The tested binding energy range from -1 MHz to -100 GHz corresponds to R_C between over $1000a_0$ and $25a_0$ and allows us to demonstrate the crossover between the asymptotic long-range and short-range models and their limitations. The transition between the long-range and short-range models being correct occurs for the range of binding energies where the Condon points lie close to $R_{\rm vdW}$. This is related to the behavior of the ground-state scattering wave-function models and their ranges of validity: $R \gg R_{\rm vdW}$ for the asymptotic model, $R \gtrsim R_{\rm vdW}$ for the long-range model, and $R \lesssim R_{\rm vdW}$ for the short-range model [2]. The cutoff binding energy that marks the transition from short- to long-range models follows from requiring that the Condon point $R_C \approx R_{\rm vdW}$. This happens when $E_b/h \approx -C_3 R_{\rm vdW}/h \approx -2.7$ GHz [marked with an arrow in Figs. 3 and 5(a)].

In practice, the asymptotic model works for bound-state energies down to about -1 GHz. The improved modeling of the scattering wave function in the long-range model extends this to about -2 GHz. The short-range model worked well for energies between about -2 and -20 GHz. For bound states below that the contribution of the excited-state vdW interaction becomes significant and our assumption of a pure resonant-dipole excited state is no longer valid. If the scattering length a is close to $\bar{a}$ (like in ^{174}Yb) both models can slightly misplace the last node because of the influence the vdW potential on the wave function around $R_{\rm vdW}$ [2]. Figure 5(a) shows the relative errors for the three models for the example case of ^{174}Yb. The asymptotic model matches the numerical calculations to within 10% for bound-state energies down to about -200 MHz; the long-range model, again, has an extended region of applicability. Away from nodes the short-range model is correct to within about 20% for bound-state energies from about -2 GHz to about -20 GHz.

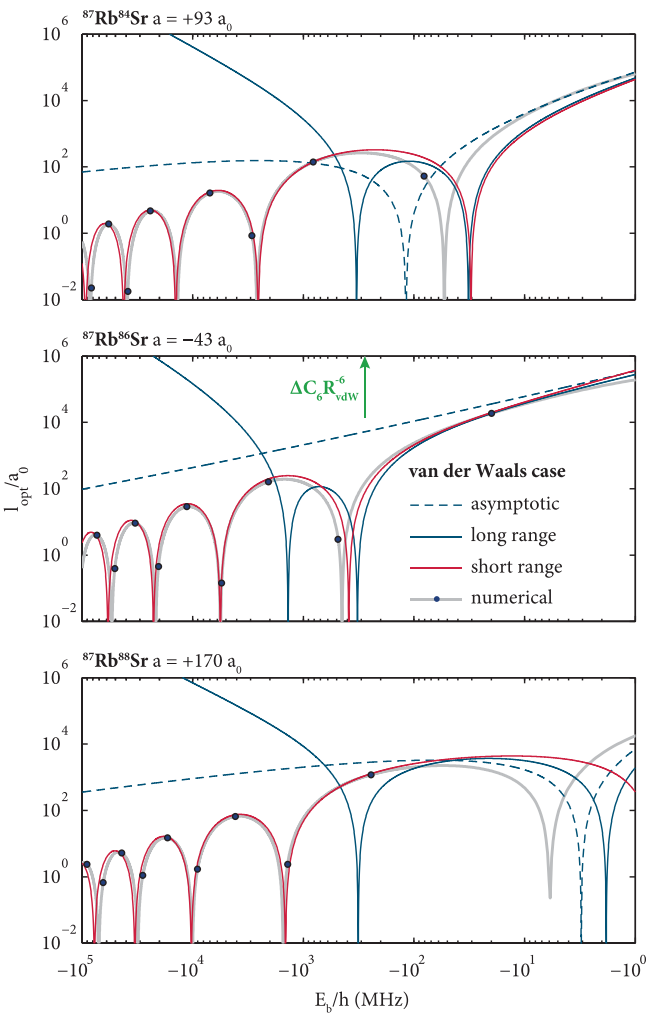

FIG. 4. Optical lengths in a van der Waals system on the example of RbSr OFRs near the Rb $D1$ line. Here all of the numerical values are satisfactorily reproduced by the short-range model (22c). The asymptotic and long-range models (22a) and (22b), respectively, are applicable only to very weakly bound states. This is easily explained by pointing out that the outer turning points for almost all excited states lie inward of $R_{\rm vdW}$, where only the short-range WKB ground-state wave function is applicable. An error plot for the ^{87}Rb^{86}Sr case in the middle panel is shown in Fig. 5(b).

B. A van der Waals case: Rb $D1$-line photoassociation of RbSr

As an example of a system with a van der Waals–dominated excited state we pick photoassociation of Rb and Sr atoms near rubidium's 795-nm $^2S_{1/2} \to {}^2P_{1/2}$ $D1$ transition [46]. There is only one Hund's case (c) molecular potential near the $^2P_{1/2} + {}^1S_0$ asymptote of RbSr, with total electronic angular momentum $j = \frac{1}{2}$ and projection $|\Omega| = \frac{1}{2}$. The case (c) long-range interaction coefficient $C_6^e(|\Omega| = \frac{1}{2})$ can be expressed [23] using interaction coefficients for the $^1S + {}^2P$ Hund's case (a) Σ and Π curves,

$$C_6^e(|\Omega| = \tfrac{1}{2}) = \tfrac{1}{3}C_6^e(^2\Sigma) + \tfrac{2}{3}C_6^e(^2\Pi), \tag{24}$$

with the coefficients for the $^2\Sigma$ and $^2\Pi$ states equal to 23 324 and 8436 atomic units, respectively. Importantly, the resultant effective $C_6^e(|\Omega| = \frac{1}{2}) = 13\,399$ a.u. is over three times larger than the van der Waals coefficient in the ground state, $C_6^g = 3686E_h a_0^6$ [15]. Having the van der Waals coefficient of the excited state much larger than that in the ground state is a prerequisite for using the stationary phase approximation (11). The breakdown of this approximation when the two interaction coefficients are of similar magnitude is described in detail in Ref. [34].

To calculate the optical lengths in this system numerically we used the recent empirical Lennard $-$ Jones $+ C_8$ ground-state potential [15] with $C_6^g \approx 3686E_h a_0^6$ and $C_8^g \approx (4.64 \times 10^5)E_h a_0^8$, whereas for the $j = \frac{1}{2}$ and $\Omega = \frac{1}{2}$ excited state we used a Lennard-Jones potential whose depth matches that

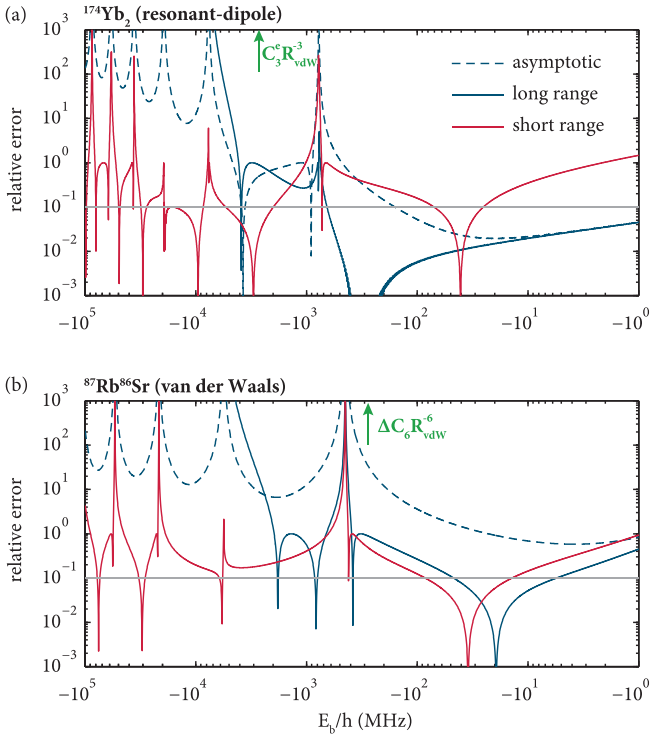

FIG. 5. Example relative errors of approximate formulas for the optical lengths of Feshbach resonances for ^{174}Yb as a representative example of (a) a resonant-dipole system and (b) a van der Waals system ^{87}Rb^{86}Sr. The blue dashed lines represent the asymptotic models and blue solid lines represent the long-range model. The red solid lines denote the short-range models. Finally, the horizontal gray lines mark a 10% error.

of the *ab initio* (2) $\Omega = \frac{1}{2}$ potential in [46]. We assumed the ground-state collision to be dominated by the s wave, with no rotational factor in the interaction potential, and we assumed transitions to the rotationless $J = \frac{1}{2}$ excited state [23]. The parameters required to use the approximate formulas (22a)–(22c) are as follows. The scattering lengths for ^{87}Rb paired with ^{84}Sr, ^{86}Sr, and ^{88}Sr are $93a_0$, $-43a_0$, and $170a_0$ [15,68], respectively, $R_{vdW} \approx 77.5a_0$, $\bar{a} \approx 74a_0$, and finally the rotational Hönl-London factor is $f_{rot} = 1$ [23].

Figure 4 shows the numerically calculated optical lengths for three isotopic combinations of the RbSr system and their approximate counterparts. Unlike the resonant-dipole example in the preceding section, here the short-range model describes virtually all resonances from the dissociation limit down to $E_b/h \approx -50$ GHz. The utility of the long-range and asymptotic models is limited, as for transitions to most bound states the Condon point R_C lies at much shorter internuclear separations than the van der Waals radius R_{vdW}. In fact, for RbSr a Condon point at $R_{vdW} \approx 77.5a_0$ corresponds to an excited-state binding energy of only about $-\Delta C_6 R_{vdW}^{-6}/h = -290$ MHz [Figs. 4 and 5(b)]. van der Waals systems usually have at most one or two bound states this close to the dissociation limit, so we expect the long-range model to occasionally be applicable to the most weakly bound state in a van der Waals system. Figure 5(b) shows the relative errors of each of the approximate formulas. Compared to the resonant-dipole example, here the formulas are more qualitative. While the short-range formula still reproduces the numerical results to within about 30% (away from nodes), the long-range model fails below about -300 MHz and the asymptotic model fails everywhere.

IV. OPTICAL LENGTH IN THE CONTEXT OF ASSOCIATIVE STIMULATED RAMAN ADIABATIC PASSAGE

A. Relationship between the optical length and free-bound transitions in a 3D optical lattice site

The utility of l_{opt} can be extended to coherent molecule production via associative stimulated Raman adiabatic passage (STIRAP) [69–71] in a doubly occupied Mott insulator [47,48]. Here we will give an expression for the free-bound Rabi frequency Ω_{FB}, induced when a laser couples an initially unbound atomic pair in a 3D optical lattice site to an excited molecular state, in terms of l_{opt}. This is useful as Ω_{FB} depends on both the molecular physics and the trap parameters, while l_{opt} is an intrinsically molecular quantity. For an atomic pair with similar masses and trapping frequencies ω_{trap} the center of mass and relative motion separate [72,73]. The latter is governed by a radial Schrödinger equation for the previous potential $V_g(R)$, but with an added harmonic potential $V_{ho}(R) = \frac{1}{2}\mu\omega_{trap}^2 R^2$. The weak trapping potential quantizes the scattering continuum into discrete trap states separated by approximately $2\hbar\omega_{trap}$ and whose positions are the solutions of [72–75]

$$\frac{1}{2}\frac{\Gamma(1/4 - e/2)}{\Gamma(3/4 - e/2)} = \frac{a}{\beta_{ho}}, \tag{25}$$

where $e = E_{trap}/\hbar\omega_{trap}$ and $\beta_{ho} = \sqrt{\hbar/\mu\omega_{trap}}$ is a characteristic length associated with the harmonic trap potential, typically on the order of $10^3 a_0$–$10^4 a_0$.

In analogy to the OFR stimulated width $\hbar\Gamma_{stim} = 2\pi|\langle f_g|V^{opt}|\psi_b\rangle|^2$, the free-bound Rabi frequency may be defined as $\hbar\Omega_{FB} = |\langle\psi_{trap}|V^{opt}|\psi_b\rangle|$, where ψ_{trap} is the trap state wave function and V^{opt} is the optical coupling matrix element [50,53]. At internuclear distances that contribute to the Franck-Condon factor (typically much shorter than β_{ho}), the trapping potential is weak compared to the trap state energy. Since ψ_{trap} and f_g are the solutions of radial Schrödinger equations that differ only by the weak harmonic potential that vanishes for small R, the trap wave function can be approximated to within a scaling factor by the scattering wave function calculated for the trap state energy. The scaling factor can be taken from multichannel quantum defect theory [49,50], $\psi_{trap} = (\partial E_{trap}/\partial\nu)^{1/2} f_g(k_{trap})$, where $(\partial E_{trap}/\partial\nu)$ is the trap state spacing. Finally, we recall the relationship between the stimulated width and the optical length $\Gamma_{stim} = 2k_{trap} l_{opt}\gamma_m$ for the wave number $k_{trap} = \sqrt{2\mu E_{trap}}/\hbar$. As a result,

$$\Omega_{FB} = \left(\frac{1}{2\pi\hbar}\frac{\partial E_{trap}}{\partial\nu} 2k_{trap} l_{opt}\gamma_m\right)^{1/2}. \tag{26}$$

In a Mott insulator [48] the atoms occupy the lowest trap state above the dissociation limit, so we use $k_{trap} = \sqrt{2e_0}/\beta_{ho}$ and $(\partial E_{trap}/\partial\nu) \approx \hbar\omega_{trap}(e_1 - e_0)$, where e_0 and e_1 are the two

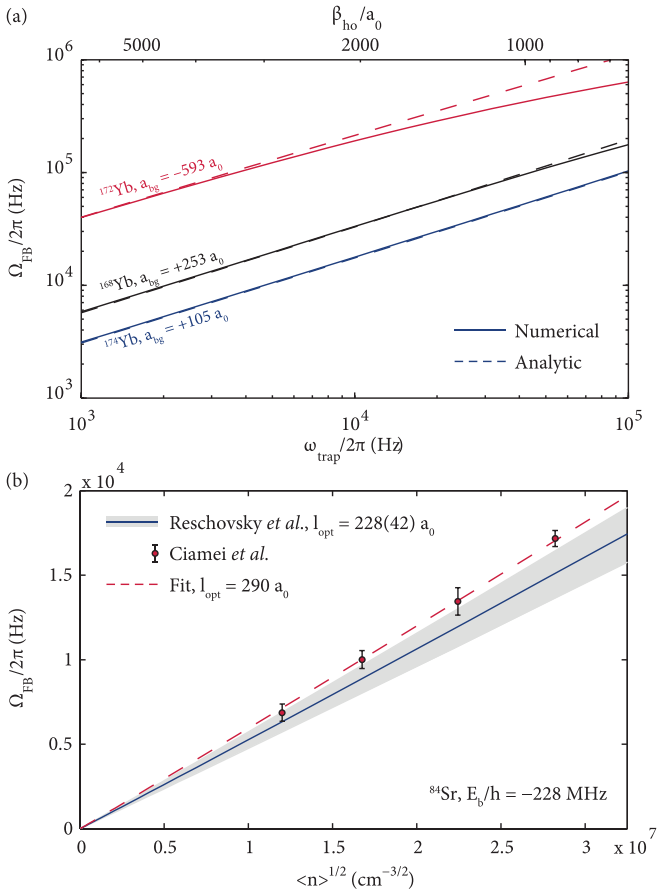

FIG. 6. Calculation of free-bound Rabi frequencies Ω_{FB} from the optical length (for $I = 1\ \mathrm{W/cm^2}$). (a) Numerical and analytic [Eq. (26)] Rabi frequencies for transitions to $^1S_0 + {}^3P_1$ states at -310, -353, and -303 MHz in ^{168}Yb, ^{172}Yb, and ^{174}Yb, respectively, as a function of trapping frequency ω_{trap}. Equation (26) remains accurate as long as $a \ll \beta_{\mathrm{ho}}$ (alternative axis). (b) Plot of Ω_{FB} for the -228-MHz $^1S_0 + {}^3P_1$ state in ^{84}Sr as a function of $\langle n\rangle^{1/2}$. Data points were measured by Ciamei *et al.* [48] and the shaded area was calculated from $l_{\mathrm{opt}} = 228(42)a_0$ measured by Reschovsky *et al.* [13].

lowest solutions of Eq. (25). We stress that this derivation does not need any of the assumptions we previously made for our approximate formulas for l_{opt}, but only that β_{ho} is much larger than any other length scale, particularly a.

B. Results

Numerical testing for Yb shows that for typical trap frequencies Eq. (26) works with an accuracy better than 10% unless a is appreciable compared to β_{ho} [Fig. 6(a)]. In ^{174}Yb characterized by a moderate scattering length of $a = 105a_0$, the agreement is to better than 2% for all tested ω_{trap}. In fact, as long as $|a/\beta_{\mathrm{ho}}| \leqslant 0.1$, this accuracy is retained for all tested isotopes. If the scattering length is resonant, as in ^{172}Yb ($a = -593a_0$), our model becomes less accurate: For a trapping frequency of $2\pi \times 10$ kHz ($|a/\beta_{\mathrm{ho}}| \approx 0.3$) the accuracy deteriorates to about 10%.

Recent experimental investigations of associative STIRAP in an ^{84}Sr Mott insulator by Ciamei *et al.* [48] and, independently, of photoassociation rates in an ^{84}Sr BEC in a dipole trap by Reschovsky *et al.* [13] allow for a real-world test of Eq. (26). Ciamei *et al.* measured Ω_{FB} for transitions to the -228 MHz state near the $^1S_0 + {}^3P_1$ asymptote in $^{84}Sr_2$ [Fig. 6(b)] and found the Rabi frequency to be proportional to the square root of the single-atom average on-site density $\langle n\rangle = 1/(2\pi)^{3/2}a_{\mathrm{ho}}^3$, where $a_{\mathrm{ho}} = \sqrt{\hbar/m\omega_{\mathrm{trap}}} = \beta_{\mathrm{ho}}/\sqrt{2}$. Indeed, aside from the weak dependence of reduced trap energies on the scattering length, the trap state spacing $\partial E/\partial n \propto \omega_{\mathrm{trap}}$, the wave number $k_{\mathrm{trap}} \propto \omega_{\mathrm{trap}}^{1/2}$, and therefore the free-bound Rabi frequency $\Omega_{\mathrm{FB}} \propto l_{\mathrm{opt}}^{1/2}\omega_{\mathrm{trap}}^{3/4} \propto l_{\mathrm{opt}}^{1/2}\langle n\rangle^{1/2}$. By fitting Eq. (26) to the measured Ω_{FB} we extract the optical length $l_{\mathrm{opt}} = 290(13)a_0$. Here $a = 122.7a_0$ [76] and $\gamma_m = 2 \times 2\pi \times 7.5$ kHz [11,77]; parentheses indicate the statistical fit uncertainty. The extracted optical length agrees to within 1.4 mutual σ with the experimental $l_{\mathrm{opt}} = 228(42)a_0$ measured by Reschovsky *et al.* [13]. Additionally, theoretical Ω_{FB} calculated using the optical length of Reschovsky *et al.* [shaded area in Fig. 6(b)] generally reproduce the measured Ω_{FB}.

V. CONCLUSION

We have developed simple analytic formulas for the optical Feshbach resonance strength parameter, the optical length, for near-threshold bound states using the stationary phase approximation [34–36,40,50]. We rely on the excited-state potential being dominated by either a resonant-dipole R^{-3} interaction typical for homonuclear photoassociation near strong lines or a van der Waals R^{-6} tail appropriate for heteronuclear systems. The optical length is expressed in terms of dominant interaction parameters and the s-wave scattering length. We have demonstrated our model using Yb_2 and RbSr as real-world examples and found semiquantitative agreement for resonances up to tens of gigahertz from the dissociation limit. The derived expressions could aid the design of future photoassociation or OFR experiments when only the long-range interaction parameters are known. The formulas could also potentially be used to determine the scattering length from experimental spectra if a more accurate method like two-color photoassociation spectroscopy is not available or practical. The resonant-dipole formulas will work for homonuclear OFRs near any allowed atomic transition, but have worked well for intercombination line OFRs in Yb [12,44,45] and should apply to thus far unexplored systems with similarly strong intercombination lines, particularly Hg [78–80] and Cd [81–84], considered as references in optical lattice clocks.

We have also shown how the optical l_{opt} may be used in the context of coherent molecular formation via associative STIRAP in a 3D optical lattice [48,71] as a measure of transition strength that is independent of trap parameters. We have found the pump beam Rabi frequency Ω_{FB} to be proportional to $l_{\mathrm{opt}}^{1/2}$ and approximately proportional to on-site density $\langle n\rangle^{1/2}$ corroborating the empirical observation of Ciamei *et al.* [48] for the $^1S_0 + {}^3P_1$ 0_u^+ -228-MHz resonance near the intercombination line in ^{84}Sr. From their experimental Ω_{FB} we extracted a value of $l_{\mathrm{opt}} = 290(13)a_0$, which agrees with an independently measured $l_{\mathrm{opt}} = 228(42)a_0$ of Reschovsky *et al.* [13].

ACKNOWLEDGMENTS

I would like to thank Piotr Żuchowski, Roman Ciuryło, Paul S. Julienne, and Alessio Ciamei for useful discussions. I acknowledge support from the National Science Centre (Grant No. 2017/25/B/ST4/01486). This work is part of an ongoing research program of the National Laboratory FAMO in Toruń, Poland. Calculations have been carried out at the Wroclaw Centre for Networking and Supercomputing through Grant No. 353.

[1] C. Chin, R. Grimm, P. Julienne, and E. Tiesinga, Feshbach resonances in ultracold gases, Rev. Mod. Phys. **82**, 1225 (2010).

[2] K. M. Jones, E. Tiesinga, P. D. Lett, and P. S. Julienne, Ultracold photoassociation spectroscopy: Long-range molecules and atomic scattering, Rev. Mod. Phys. **78**, 483 (2006).

[3] H. R. Thorsheim, J. Weiner, and P. S. Julienne, Laser-Induced Photoassociation of Ultracold Sodium Atoms, Phys. Rev. Lett. **58**, 2420 (1987).

[4] P. D. Lett, K. Helmerson, W. D. Phillips, L. P. Ratliff, S. L. Rolston, and M. E. Wagshul, Spectroscopy of Na_2 by Photoassociation of Laser-Cooled Na, Phys. Rev. Lett. **71**, 2200 (1993).

[5] J. D. Miller, R. A. Cline, and D. J. Heinzen, Photoassociation Spectrum of Ultracold Rb Atoms, Phys. Rev. Lett. **71**, 2204 (1993).

[6] L. P. Ratliff, M. E. Wagshul, P. D. Lett, S. L. Rolston, and W. D. Phillips, Photoassociative spectroscopy of 1_g, 0_u^+, and 0_g^- states of Na_2, J. Chem. Phys. **101**, 2638 (1994).

[7] G. Zinner, T. Binnewies, F. Riehle, and E. Tiemann, Photoassociation of Cold Ca Atoms, Phys. Rev. Lett. **85**, 2292 (2000).

[8] T. Zelevinsky, M. M. Boyd, A. D. Ludlow, T. Ido, J. Ye, R. Ciuryło, P. Naidon, and P. S. Julienne, Narrow Line Photoassociation in an Optical Lattice, Phys. Rev. Lett. **96**, 203201 (2006).

[9] M. Borkowski, R. Ciuryło, P. S. Julienne, R. Yamazaki, H. Hara, K. Enomoto, S. Taie, S. Sugawa, Y. Takasu, and Y. Takahashi, Photoassociative production of ultracold heteronuclear ytterbium molecules, Phys. Rev. A **84**, 030702(R) (2011).

[10] Y. Takasu, Y. Saito, Y. Takahashi, M. Borkowski, R. Ciuryło, and P. S. Julienne, Controlled Production of Subradiant States of a Diatomic Molecule in an Optical Lattice, Phys. Rev. Lett. **108**, 173002 (2012).

[11] M. Borkowski, P. Morzyński, R. Ciuryło, P. S. Julienne, M. Yan, B. J. DeSalvo, and T. C. Killian, Mass scaling and nonadiabatic effects in photoassociation spectroscopy of ultracold strontium atoms, Phys. Rev. A **90**, 032713 (2014).

[12] M.-S. Kim, J. Lee, J. H. Lee, Y. Shin, and J. Mun, Measurements of optical Feshbach resonances of ^{174}Yb atoms, Phys. Rev. A **94**, 042703 (2016).

[13] B. J. Reschovsky, B. P. Ruzic, H. Miyake, N. C. Pisenti, P. S. Julienne, and G. K. Campbell, Narrow-line photoassociation spectroscopy and mass-scaling of bosonic strontium, arXiv:1808.06507.

[14] F. Münchow, C. Bruni, M. Madalinski, and A. Görlitz, Two-photon photoassociation spectroscopy of heteronuclear YbRb, Phys. Chem. Chem. Phys. **13**, 18734 (2011).

[15] A. Ciamei, J. Szczepkowski, A. Bayerle, V. Barbé, L. Reichsöllner, S. M. Tzanova, C.-C. Chen, B. Pasquiou, A. Grochola, P. Kowalczyk, W. Jastrzebski, and F. Schreck, The RbSr $^2\Sigma^+$ ground state investigated via spectroscopy of hot and ultracold molecules, Phys. Chem. Chem. Phys. **20**, 26221 (2018).

[16] R. Roy, R. Shrestha, A. Green, S. Gupta, M. Li, S. Kotochigova, A. Petrov, and C. H. Yuen, Photoassociative production of ultracold heteronuclear YbLi* molecules, Phys. Rev. A **94**, 033413 (2016).

[17] A. Guttridge, S. A. Hopkins, M. D. Frye, J. J. McFerran, J. M. Hutson, and S. L. Cornish, Production of ultracold Cs*Yb molecules by photoassociation, Phys. Rev. A **97**, 063414 (2018).

[18] G. Reinaudi, C. B. Osborn, M. McDonald, S. Kotochigova, and T. Zelevinsky, Optical Production of Stable Ultracold $^{88}Sr_2$ Molecules, Phys. Rev. Lett. **109**, 115303 (2012).

[19] J. M. Sage, S. Sainis, T. Bergeman, and D. DeMille, Optical Production of Ultracold Polar Molecules, Phys. Rev. Lett. **94**, 203001 (2005).

[20] J. Deiglmayr, A. Grochola, M. Repp, K. Mörtlbauer, C. Glück, J. Lange, O. Dulieu, R. Wester, and M. Weidemüller, Formation of Ultracold Polar Molecules in the Rovibrational Ground State, Phys. Rev. Lett. **101**, 133004 (2008).

[21] G. Quéméner and P. S. Julienne, Ultracold Molecules under Control!, Chem. Rev. **112**, 4949 (2012).

[22] C. D. Bruzewicz, M. Gustavsson, T. Shimasaki, and D. DeMille, Continuous formation of vibronic ground state RbCs molecules via photoassociation, New J. Phys. **16**, 023018 (2014).

[23] M. Borkowski, R. Muñoz Rodriguez, M. B. Kosicki, R. Ciuryło, and P. S. Żuchowski, Optical Feshbach resonances and ground state molecule production in the RbHg system, Phys. Rev. A **96**, 063411 (2017).

[24] P. O. Fedichev, Y. Kagan, G. V. Shlyapnikov, and J. T. M. Walraven, Influence of Nearly Resonant Light on the Scattering Length in Low-Temperature Atomic Gases, Phys. Rev. Lett. **77**, 2913 (1996).

[25] J. L. Bohn and P. S. Julienne, Prospects for influencing scattering lengths with far-off-resonant light, Phys. Rev. A **56**, 1486 (1997).

[26] F. K. Fatemi, K. M. Jones, and P. D. Lett, Observation of Optically Induced Feshbach Resonances in Collisions of Cold Atoms, Phys. Rev. Lett. **85**, 4462 (2000).

[27] M. Theis, G. Thalhammer, K. Winkler, M. Hellwig, G. Ruff, R. Grimm, and J. H. Denschlag, Tuning the Scattering Length with an Optically Induced Feshbach Resonance, Phys. Rev. Lett. **93**, 123001 (2004).

[28] G. Thalhammer, M. Theis, K. Winkler, R. Grimm, and J. H. Denschlag, Inducing an optical Feshbach resonance via stimulated Raman coupling, Phys. Rev. A **71**, 033403 (2005).

[29] K. Enomoto, K. Kasa, M. Kitagawa, and Y. Takahashi, Optical Feshbach Resonance Using the Intercombination Transition, Phys. Rev. Lett. **101**, 203201 (2008).

[30] R. Yamazaki, S. Taie, S. Sugawa, and Y. Takahashi, Submicron Spatial Modulation of an Interatomic Interaction in a Bose-Einstein Condensate, Phys. Rev. Lett. **105**, 050405 (2010).

[31] S. Blatt, T. L. Nicholson, B. J. Bloom, J. R. Williams, J. W. Thomsen, P. S. Julienne, and J. Ye, Measurement of Optical Feshbach Resonances in an Ideal Gas, Phys. Rev. Lett. **107**, 073202 (2011).

[32] M. Yan, B. J. DeSalvo, B. Ramachandhran, H. Pu, and T. C. Killian, Controlling Condensate Collapse and Expansion with an Optical Feshbach Resonance, Phys. Rev. Lett. **110**, 123201 (2013).

[33] R. Ciuryło, E. Tiesinga, and P. S. Julienne, Optical tuning of the scattering length of cold alkaline-earth-metal atoms, Phys. Rev. A **71**, 030701(R) (2005).

[34] R. Ciuryło, E. Tiesinga, and P. S. Julienne, Stationary phase approximation for the strength of optical Feshbach resonances, Phys. Rev. A **74**, 022710 (2006).

[35] A. Jabloński, General theory of pressure broadening of spectral lines, Phys. Rev. **68**, 78 (1945).

[36] P. S. Julienne, Cold binary atomic collisions in a light field, J. Res. Natl. Inst. Stand. Technol. **101**, 487 (1996).

[37] B. R. Johnson, New numerical methods applied to solving the one-dimensional eigenvalue problem, J. Chem. Phys. **67**, 4086 (1977).

[38] D. T. Colbert, W. H. Miller, D. T. Colbert, and W. H. Miller, A novel discrete variable representation for quantum mechanical reactive scattering via the *S*-matrix Kohn method, J. Chem. Phys. **96**, 1982 (1992).

[39] E. Tiesinga, C. J. Williams, and P. S. Julienne, Photoassociative spectroscopy of highly excited vibrational levels of alkali-metal dimers: Green-function approach for eigenvalue solvers, Phys. Rev. A **57**, 4257 (1998).

[40] C. Boisseau, E. Audouard, J. Vigué, and P. S. Julienne, Reflection approximation in photoassociation spectroscopy, Phys. Rev. A **62**, 052705 (2000).

[41] G. F. Gribakin and V. V. Flambaum, Calculation of the scattering length in atomic collisions using the semiclassical approximation, Phys. Rev. A **48**, 546 (1993).

[42] B. J. Verhaar, E. G. M. van Kempen, and S. J. J. M. F. Kokkelmans, Predicting scattering properties of ultracold atoms: Adiabatic accumulated phase method and mass scaling, Phys. Rev. A **79**, 032711 (2009).

[43] M. Borkowski, P. S. Żuchowski, R. Ciuryło, P. S. Julienne, D. Kędziera, Ł. Mentel, P. Tecmer, F. Münchow, C. Bruni, and A. Görlitz, Scattering lengths in isotopologues of the RbYb system, Phys. Rev. A **88**, 052708 (2013).

[44] S. Tojo, M. Kitagawa, K. Enomoto, Y. Kato, Y. Takasu, M. Kumakura, and Y. Takahashi, High-Resolution Photoassociation Spectroscopy of Ultracold Ytterbium Atoms by Using the Intercombination Transition, Phys. Rev. Lett. **96**, 153201 (2006).

[45] M. Borkowski, R. Ciuryło, P. S. Julienne, S. Tojo, K. Enomoto, and Y. Takahashi, Line shapes of optical Feshbach resonances near the intercombination transition of bosonic ytterbium, Phys. Rev. A **80**, 012715 (2009).

[46] A. Devolder, E. Luc-Koenig, O. Atabek, M. Desouter-Lecomte, and O. Dulieu, Proposal for the formation of ultracold deeply bound RbSr dipolar molecules by all-optical methods, Phys. Rev. A **98**, 053411 (2018).

[47] S. Stellmer, B. Pasquiou, R. Grimm, and F. Schreck, Creation of Ultracold Sr_2 Molecules in the Electronic Ground State, Phys. Rev. Lett. **109**, 115302 (2012).

[48] A. Ciamei, A. Bayerle, C.-C. Chen, B. Pasquiou, and F. Schreck, Efficient production of long-lived ultracold Sr_2 molecules, Phys. Rev. A **96**, 013406 (2017).

[49] F. H. Mies, A multichannel quantum defect analysis of diatomic predissociation and inelastic atomic scattering, J. Chem. Phys. **80**, 2514 (1984).

[50] J. L. Bohn and P. S. Julienne, Semianalytic theory of laser-assisted resonant cold collisions, Phys. Rev. A **60**, 414 (1999).

[51] R. J. Le Roy and R. B. Bernstein, Dissociation energy and long-range potential of diatomic molecules from vibrational spacings of higher levels, J. Chem. Phys. **52**, 3869 (1970).

[52] M. Yan, B. J. DeSalvo, Y. Huang, P. Naidon, and T. C. Killian, Rabi Oscillations between Atomic and Molecular Condensates Driven with Coherent One-Color Photoassociation, Phys. Rev. Lett. **111**, 150402 (2013).

[53] T. L. Nicholson, S. Blatt, B. J. Bloom, J. R. Williams, J. W. Thomsen, J. Ye, and P. S. Julienne, Optical Feshbach resonances: Field-dressed theory and comparison with experiments, Phys. Rev. A **92**, 022709 (2015).

[54] R. Napolitano, J. Weiner, and P. S. Julienne, Theory of optical suppression of ultracold-collision rates by polarized light, Phys. Rev. A **55**, 1191 (1997).

[55] M. Machholm, P. S. Julienne, and K.-A. Suominen, Calculations of collisions between cold alkaline-earth-metal atoms in a weak laser field, Phys. Rev. A **64**, 033425 (2001).

[56] R. Ciuryło, E. Tiesinga, S. Kotochigova, and P. S. Julienne, Photoassociation spectroscopy of cold alkaline-earth-metal atoms near the intercombination line, Phys. Rev. A **70**, 062710 (2004).

[57] J. M. Brown and A. Carrington, *Rotational Spectroscopy of Diatomic Molecules* (Cambridge University Press, Cambridge, 2003).

[58] R. Le Roy, in *Molecular Spectroscopy*, edited by R. F. Barrow, D. A. Long, and D. J. Millen (Royal Society of Chemistry, Cambridge, 1973), pp. 113–171.

[59] E. P. Wigner, On the behavior of cross sections near thresholds, Phys. Rev. **73**, 1002 (1948).

[60] K. M. Jones, P. D. Lett, E. Tiesinga, and P. S. Julienne, Fitting line shapes in photoassociation spectroscopy of ultracold atoms: A useful approximation, Phys. Rev. A **61**, 012501 (1999).

[61] M. Kitagawa, K. Enomoto, K. Kasa, Y. Takahashi, R. Ciuryło, P. Naidon, and P. S. Julienne, Two-color photoassociation spectroscopy of ytterbium atoms and the precise determinations of *s*-wave scattering lengths, Phys. Rev. A **77**, 012719 (2008).

[62] M. Borkowski, A. A. Buchachenko, R. Ciuryło, P. S. Julienne, H. Yamada, Y. Kikuchi, K. Takahashi, Y. Takasu, and Y. Takahashi, Beyond-Born-Oppenheimer effects in sub-kHz-precision photoassociation spectroscopy of ytterbium atoms, Phys. Rev. A **96**, 063405 (2017).

[63] P. S. Julienne and F. H. Mies, Collisions of ultracold trapped atoms, J. Opt. Soc. Am. B **6**, 2257 (1989).

[64] F. H. Mies and M. Raoult, Analysis of threshold effects in ultracold atomic collisions, Phys. Rev. A **62**, 012708 (2000).

[65] J. J. Lutz and J. M. Hutson, Deviations from Born-Oppenheimer mass scaling in spectroscopy and ultracold molecular physics, J. Mol. Spectrosc. **330**, 43 (2016).

[66] A. A. Buchachenko, G. Chałasiński, and M. M. Szczęśniak, Interactions of lanthanide atoms: Comparative *ab initio* study of YbHe, Yb_2 and TmHe, TmYb potentials, Eur. Phys. J. D **45**, 147 (2007).

[67] F. H. Mies, W. J. Stevens, and M. Krauss, Model calculation of the electronic structure and spectroscopy of Hg_2, J. Mol. Spectrosc. **72**, 303 (1978).

[68] V. Barbé, A. Ciamei, B. Pasquiou, L. Reichsöllner, F. Schreck, P. S. Żuchowski, and J. M. Hutson, Observation of Feshbach resonances between alkali and closed-shell atoms, Nat. Phys. **14**, 881 (2018).

[69] K. Bergmann, H. Theuer, and B. W. Shore, Coherent population transfer among quantum states of atoms and molecules, Rev. Mod. Phys. **70**, 1003 (1998).

[70] K. K. Ni, S. Ospelkaus, M. H. De Miranda, A. Pe'er, B. Neyenhuis, J. J. Zirbel, S. Kotochigova, P. S. Julienne, D. S. Jin, and J. Ye, A high phase-space-density gas of polar molecules, Science **322**, 231 (2008).

[71] N. V. Vitanov, A. A. Rangelov, B. W. Shore, and K. Bergmann, Stimulated Raman adiabatic passage in physics, chemistry, and beyond, Rev. Mod. Phys. **89**, 015006 (2017).

[72] T. Busch, B.-G. Englert, K. Rzążewski, and M. Wilkens, Two cold atoms in a harmonic trap, Found. Phys. **28**, 549 (1998).

[73] Y. Chen and B. Gao, Multiscale quantum-defect theory for two interacting atoms in a symmetric harmonic trap, Phys. Rev. A **75**, 053601 (2007).

[74] M. Block and M. Holthaus, Pseudopotential approximation in a harmonic trap, Phys. Rev. A **65**, 052102 (2002).

[75] S. Shresta, E. Tiesinga, and C. Williams, Scattering-length determination from trapped pairs of atoms, Phys. Rev. A **72**, 022701 (2005).

[76] Y. N. Martinez de Escobar, P. G. Mickelson, P. Pellegrini, S. B. Nagel, A. Traverso, M. Yan, R. Côté, and T. C. Killian, Two-photon photoassociative spectroscopy of ultracold ^{88}Sr, Phys. Rev. A **78**, 062708 (2008).

[77] W. Skomorowski, F. Pawłowski, C. P. Koch, and R. Moszynski, Rovibrational dynamics of the strontium molecule in the $A\,^1\Sigma_u^+$, $c\,^3\Pi_u$, and $a\,^3\Sigma_u^+$ manifold from state-of-the-art *ab initio* calculations, J. Chem. Phys. **136**, 194306 (2012).

[78] M. Krośnicki, M. Strojecki, T. Urbańczyk, A. Pashov, and J. Koperski, Interatomic potentials of the heavy van der Waals dimer Hg_2: A "test-bed" for theory-to-experiment agreement, Phys. Rep. **591**, 1 (2015).

[79] K. Yamanaka, N. Ohmae, I. Ushijima, M. Takamoto, and H. Katori, Frequency Ratio of ^{199}Hg and ^{87}Sr Optical Lattice Clocks Beyond the SI Limit, Phys. Rev. Lett. **114**, 230801 (2015).

[80] R. Tyumenev, M. Favier, S. Bilicki, E. Bookjans, R. L. Targat, J. Lodewyck, D. Nicolodi, Y. L. Coq, M. Abgrall, J. Guéna, L. D. Sarlo, and S. Bize, Comparing a mercury optical lattice clock with microwave and optical frequency standards, New J. Phys. **18**, 113002 (2016).

[81] P. Masłowski, K. Bielska, A. Cygan, J. Domysławska, D. Lisak, R. Ciuryło, A. Bielski, and R. S. Trawiński, The hyperfine and isotope structure of the Cd intercombination line–revisited, Eur. Phys. J. D **51**, 295 (2009).

[82] T. Urbańczyk, M. Strojecki, M. Krośnicki, A. Kędziorski, P. S. Żuchowski, and J. Koperski, Interatomic potentials of metal dimers: Probing agreement between experiment and advanced *ab initio* calculations for van der Waals dimer Cd_2, Int. Rev. Phys. Chem. **36**, 541 (2017).

[83] A. Yamaguchi, M. S. Safronova, K. Gibble, and H. Katori, Narrow-Line Cooling and Determination of the Magic Wavelength of Cd, Phys. Rev. Lett. **123**, 113201 (2019).

[84] V. A. Dzuba and A. Derevianko, Blackbody radiation shift for the $^1S_0$-$^3P_0$ optical clock transition in zinc and cadmium atoms, J. Phys. B **52**, 215005 (2019).